CNT/PDMS composite membranes for H_2 and CH_4 gas separation

Majid Nour [a,d*], Kyle Berean [a,d*], Sivacarendran Balendhran [a,d], Jian Zhen Ou [a], Johan Du Plessis [b], Chris McSweeney [c], Madhu Bhaskaran [a,d], Sharath Sriram [a,d], and Kourosh Kalantar-zadeh[a,d]*

[a] School of Electrical and Computer Engineering, RMIT University, Melbourne, Australia

[b] School of Applied Sciences, RMIT University, Melbourne, Australia

[c] CSIRO Livestock Industries, Queensland BioScience Precinct, St Lucia, Australia

[d] Functional Materials and Microsystems Research Group, RMIT University, Melbourne, Australia

* Corresponding authors. E-mail: nour.mk@gmail.com (M. Nour), kyleberean@gmail.com (K. Berean), and kourosh.kalantar@rmit.edu.au (K. Kalantar-zadeh)

Abstract

Polydimethylsiloxane (PDMS) composites with different weight amounts of multi-walled carbon nanotubes (MWCNT) were synthesised as membranes to evaluate their gas separation properties. The selectivity of the membranes was investigated for the separation of H_2 from CH_4 gas species. Membranes with MWCNT concentrations of 1% increased the selectivity to H_2 gas by 94.8%. Furthermore, CH_4 permeation was almost totally blocked through membranes with MWCNT concentrations greater than 5%. Vibrational spectroscopy and X-ray photoelectron spectroscopy techniques revealed that upon the incorporation of MWCNT a decrease in the number of available Si–CH_3 and Si–O bonds as well as an increase in the formation of Si–C bonds occurred that initiated the reduction in CH_4 permeation. As a result, the developed membranes can be an efficient and low cost solution for separating H_2 from larger gas molecules such as CH_4.

Keywords

Gas separation, carbon nanotube, polydimethylsiloxane, membrane, CH_4, H_2

1. Introduction

The purification of hydrogen (H_2) gas is of paramount importance for many applications. However, most of the conventional gas purification methods are costly, require bulky equipment, and demand high energies. Membrane technologies offer an alternative low cost, efficient and low energy solution for H_2 gas separation.[1, 2] The use of membranes for separating different gas species has been increasing in past few years, especially for H_2 gas separation and purification. Moreover, it has been estimated that in year 2020 the market will depend on membrane gas separation technology five times more than that of year 2000 [3]. This trend is attributed to the advantages that membrane technology possesses over others. Some of these advantages include high efficiency and stability, low energy requirement, ease of operation and mechanical robustness [4-7]. However, further growth of the market scale for gas separation membrane technology depends on the availability of new and more efficient types of selective membranes that offer unique capabilities. Hence, recent research on gas separating membranes has focussed on improving the permeability and the selectivity to specific gases by investigating the use of new materials [8-10].

Membrane-based gas separation involves a mixture of two or more gases interacting through a semipermeable barrier, allowing some components to permeate freely, whilst selectively blocking the other components [11]. It is this selective blocking that favours the application of polymer-based mixed matrix membranes (MMMs) as the transport layer. In addition, researchers have been turning to MMMs to increase the desired selectivity, while maintaining permeability for the target gas [9, 10, 12, 13].

A MMM consists of a base polymer with additive fillers. The fillers that can be added to polymer to produce the MMM can be varied for different purposes creating unique composites with the capability of tuning various properties such as robustness, conductivity,

and for the purpose of this project, gas selectivity [14, 15]. It has been shown that selectivity within a polymer can be improved using many types of fillers including metal oxides, metals as well as many other organic and inorganic fillers [12, 13, 16].

Many carbon-based fillers such as carbon black (CB), graphene, and carbon nanotubes (CNT) have been used in MMMs to evaluate their effect in changing their properties. These carbon-based fillers have been widely implemented due to their conductivity, affinity to small molecules such as H_2 and ability to endure high temperatures and aggressive chemicals [3]. Several studies have been performed on the effect of the incorporation of carbon-based fillers into polymers on the selectivity and gas separation properties, especially H_2 gas from other gas species [9, 17-19]. Our previous study showed that CB nanoparticles are attractive additives to polydimethylsiloxane (PDMS) for improving H_2/CH_4 selectivity [9]. Moreover, other studies have incorporated CNT's within different polymers, such as polyimide (PI)[18], poly(imide siloxane) [17], and polysulphone (PSF)[19], to alter their gas permeation properties, making them more selective and sensitive to target gases.

The development of a successful MMM with the desired properties depends on the proper selection of the polymer and filler materials, their structural and physiochemical properties, and the ratios of their concentrations [3]. A favourable base polymer that is commonly used for developing MMMs for gas separation is PDMS [20-22]. PDMS has been widely used for MMM applications due to its ideal properties, which include low cost, biocompatibility, nontoxicity, and ease of fabrication [20-26]. PDMS offers one of the highest permeability coefficients for a wide range of gas species and it provides a very modest selectivity [7]. This creates the opportunity to utilise fillers to provide enhanced selectivity of PDMS to target gasses.

CNT, which are graphite sheets rolled into circular bundles, have been researched extensively as filler in MMMs due to their ideal properties [27-31] with both single-walled (SW) and multi-walled (MW) versions of CNT being utilised [3, 10, 15, 32, 33]. Their extraordinary mechanical and electrical properties nominate their use as a filler to reinforce the structure of the polymer matrix or to increase the electrical conductivity of the composite materials. The nanoscale dimensions of CNT provide a large surface-to-volume ratio, and hence, increase the chances of the permeate gas molecule to interact with their surfaces [31]. CNT also have a high surface energy that can interact with most gas molecules [31]. In addition to such properties, a number of studies have confirmed that the use of CNT as a filler in different types of polymers have altered their gas separation characteristics [17-19]. For example, Sanip *et al.* [18] has embedded functionalized multi-walled CNT (MWCNT) into polyimide to separate CO_2/CH_4. Kim *et al.* coated CNT within a thin polysulfone (PSF) layer [19] and in another study demonstrated that CNT–poly(imide siloxane) MMMs have changed the permeability of CH_4 through membranes [17]. However, the aforementioned studies suffer from lack of proper characterization and analysis of the membranes operation and do not provide any in-depth understanding of the mechanisms of gas separation.

We have previously shown that at 6% of CB in PDMS, we could create a MMM which efficiently separated H_2 and CH_4 gases [9]. Based on our previous studies on CB-based PDMS MMM and the aforesaid properties of CNT, it can be hypothesised that incorporating CNT into PDMS would lead to the enhancement of the MMMs' separation ability of H_2 and CH_4 and that the separation can occur at much lower concentration of CNT.

The intention of this work is to validate these hypotheses, which will be verified by fabricating and analyzing MMMs consisting of CNT dispersed within PDMS. In addition, to identify conditions for optimum performance, MMMs with varying CNT concentrations will be prepared. The gas separation properties of these nanocomposite membranes for separating

H_2 and CH_4 gas species will be evaluated, and correlated to their chemical structure as determined by electron microscopy, vibrational spectroscopy, and X-ray photoelectron spectroscopy (XPS).

2. Materials and Methods

2.1 Membrane preparation

For the fabrication of polymer nanocomposites membranes, PDMS (Sylgard 184, Dow Corning Corporation) and MWCNT with outer diameter of 20–40 nm and length of 10–30 μm (Cheap Tubes, Inc.) were utilised. Beside a pure PDMS membrane, three different MWCNT-PDMS nanocomposite membranes were prepared with MWCNT weight percentages including 1%, 5%, and 10%. First, MWCNT's were dispersed in toluene, to facilitate effective and uniform dispersion of MWCNT within the PDMS viscous matrix. The toluene/MWCNT suspension was then added to PDMS base followed by vigorous manual mixing. The mixture was then sonicated in an ultrasonic bath for 0.5 h before being mechanically stirred for 1 h at 70 °C to evaporate the toluene solvent. Allowing the mixture to cool to room temperature, PDMS curing agent (Sylgard 184 kit, Dow Corning Corporation) was added at a weight ratio of 1:1 to the PDMS base. The mixture was stirred for 10 min before drop casting and levelling on petri dishes with dimensions of 100 mm diameter and 15 mm depth. These petri dishes were placed in vacuum oven for 1 h at 70 °C to degas and allowed to cure at room temperature for a period of 2 days. The resultant membranes had similar thicknesses of approximately 100 μm and were sectioned into 20 mm × 20 mm squares for permeability measurements.

2.2 Microstructural and spectroscopic analyses

The characterizations of pure PDMS and nanocomposite MWCNT/PDMS membranes were conducted using electron microscopy, vibrational spectroscopy, and XPS. An FEI Nova NanoSEM scanning electron microscope (SEM) was used to image and study the cross-sectional morphology of the membranes. A Thermo Nicolet 6700 spectrophotometer was used to record the Fourier transform infrared (FTIR) spectra of PDMS and MWCNT/PDMS membranes. Micro-Raman characterization of the samples was performed using a Renishaw InVia Raman spectrometer at 633 nm wavelength and 20 s exposures over 3 accumulations with a laser power of 5 mW. XPS was performed using a Thermo Scientific K-alpha instrument with an Al Kα source.

2.3 Gas sensing setup

A gas chamber setup, shown in Fig. 1, was designed and implemented to conduct measurements on the permeability and selectivity of the membranes to CH_4 and H_2. The setup was comprised of the membrane under examination, placed adjoining the main gas chamber of dimensions $17 \times 12 \times 5$ cm^3. The chamber contains a 0.5 cm radius opening with a semiconducting gas sensor fixed to the membrane outside of the chamber (see inset of Fig. 1). The sensor was housed in such a way that only the diffused gas passing through the membrane could affect its response. An accurately calibrated commercial CH_4 semiconducting gas sensor (TGS 2611, Figaro, Inc., USA) was used for monitoring the concentration of the gases diffused through the membrane. This sensor was chosen for the strong response it shows to H_2 in addition to its sensitivity to CH_4. This cross-response was desirable, making it practical for assessing the selectivity of different membranes to CH_4 and H_2. From the data sheet for TGS 2611 CH_4 sensor, the response of this device to CH_4 is approximately 1.5 times larger than its response to H_2 for the same concentration of the gases.

A mass flow controller (MKS Instruments, Inc, USA) was used to regulate the gas feed into the chamber. The sensor measurements were carried out using a custom data acquisition system using a custom design LABVIEW software-based program.

3. Results and discussions

3.1 Microstructural and spectroscopic analyses

The nanocomposite MWCNT/PDMS membranes were characterized using SEM, vibrational spectroscopy techniques and XPS to determine their properties at different MWCNT concentrations.

3.1.1 Cross-sectional electron microscopy

In order to examine the dispersion of MWCNT throughout the polymer and the morphology of the composites, SEM was used. To prevent charging of the nanocomposites under the microscope, the pure PDM and 1% samples were coated with platinum and all of the other samples images were captured at relatively low beam voltages.

Fig. 2 shows the SEM images of the fabricated MWCNT/PDMS composites (the pure PDMS SEM image is presented in *Supplementary Information* Fig. S2 for comparison). It was observed that particle dispersion was reasonably homogenous in all samples. However, some MWCNT dense areas bundles were still present in the membranes. Visually as the concentration of MWCNT increases in the membrane, its structure transformed further to a composite structure. No exceptional morphological behaviour was observed after the addition of MWCNT particles at different concentrations.

3.1.2 FTIR studies

Fig. 3 illustrates the FTIR spectra of pristine PDMS and MWCNT/PDMS composites of different concentrations (See Fig.S3 in *Supplementary Information* for the full FTIR spectra). The peaks between 1400–1420 cm^{-1} and between 1240–1280 cm^{-1} correspond to $–CH_3$ deformation vibration in PDMS [34]. The Si–O–Si stretching multi-component peaks for PDMS are observed in the range between 930 to 1200 cm^{-1}. The peaks that appear between 2100–2200 cm^{-1} are due to the formation of Si–H bond in the matrix [35]. The symmetric and asymmetric peaks that appear at 2906 cm^{-1} and 2950–2970 cm^{-1} (as can be seen in Fig. S3) are due to the $–CH_3$ stretching in $≡Si–CH_3$. It has been previously reported [34, 36, 37] that Si–C bands and $Si(CH_3)_2$ rocking peaks appear in the region of 825–865 cm^{-1} and 785–815 cm^{-1}, respectively, which are also seen in our FTIR spectra for composites. The significant difference between pure PDMS and MWCNT/PDMS composite FTIR spectra is observed at 905 cm^{-1} for which the peak becomes sharper and gains a notably lower intensity as the concentration of MWCNT increase in PDMS. This could be due to the formation of Si–C bond.

3.1.3 Raman spectroscopy studies

The pure PDMS membrane Raman spectrum presented in Fig. 4 (continuous line), contains the typical PDMS peaks, concurring with the spectra presented in previous works [36]. It comprises of a Si–O–Si symmetric peak at 488 cm^{-1} and at 607 cm^{-1} appears the $Si–CH_3$ symmetric rocking peak. The Si–C symmetric stretching appears at 708 cm^{-1} and CH_3 asymmetric rocking appears at 787 cm^{-1}. At 862 and 1262 cm^{-1}, CH_3 symmetric rocking and symmetric bending are seen, respectively [38]. Following the dispersion of MWCNT' within the MMM, we observe that the $Si–CH_3$ symmetric rocking band shift peak decreases as the concentration of MWCNT increases.

MWCNT's Raman spectra have been thoroughly studied, and have band assignments that are well established [39-41].

The Raman spectra of the MWCNT-PDMS nanocomposites show the first order carbon bands as the *D* band (disorder band) at around 1330 cm^{-1} and a wide *G* band (TM-tangential mode or graphite band) at around 1605 cm^{-1}. The two bands can be clearly seen in Fig. 4 with the *D* band showing the disorder in the graphitic structure of MWCNT [42-44]. The wide peak observed in the *G* band can be explained by the disentanglement of the MWCNT and subsequent dispersion in the PDMS matrix as an outcome of polymer infiltration into the MWCNT bundles [45]. The intensity ratio of *D* and *G* bands has been shown to be a strong indicator of the structural arrangement [39, 46]. The intensity ratios of *D* band to the *G* band ($I_D//I_G$) in the composites ranged from 1% to 10% increased from 1.59 to 1.72, respectively, showing the reduction in the order as the amount of MWCNT increases.

3.1.4 XPS studies

Fig. 5(a) and 5(d) show the C(1s) XPS spectra of the PDMS membrane and the PDMS+1% MWCNT composite, respectively. Curve fitting reveals a singular peak centred around a binding energy of approximately 284 eV, which corresponds to C–C, C=C, and C–H bonds [47, 48]. It is important to note that the C–Si bond also lies within this peak at 283.8 eV. The C(1s) peak within the pure PDMS membrane resulted in 44% of the overall binding energy, while in the nanocomposite membrane was responsible for 48% of all binding energy. This was expected with the addition of the MWCNT within the polymer matrix. The O(1s) spectrum of the PDMS and the PDMS+1% MWCNT composite presented in Fig. 5(b) and (e) show a singular peak fitted to approximately 532 eV that match up to those found in past studies [49].

It was also important to examine the Si(2p) XPS spectrum for the pure PDMS and the PDMS nanocomposite as shown in Fig. 5(c) and 5(f), respectively, to assess the type of bonds that Si atoms establish. The deconvolution of the Si(2p) spectrum results in two peaks, one occurring at 102 eV (peak *A* in Fig. 5(c) and 5(f)) ,which can be attributed to Si-O bonds within PDMS and the other at and 103.7 eV (peak *B* in Fig. 5(c) and 5(f)), which corresponds to silicon bonding to three oxygen atoms, which compares to those found in earlier reports [50, 51]. The figures show a clear reduction in the occurrence of the higher binding energy peak within the nanocomposite, when compared to the pure PDMS spectrum. This suggests that the reduction in quantity of silicon to three oxygen bonds is in response to this increase in the number of Si–C bonds occurring with the addition of MWCNT.

3.2 Gas permeability and sensitivity

The gas selectivity and permeability of the composite membranes were inspected at several concentrations of CH_4 and H_2 in ambient air, pumped through the mass flow controller setup that was presented in Section 2.3. All measurements were performed at room temperature and the commercial sensor's heater was supplied with a 5 V DC as recommended by the manufacturer. The sensor's resistance was sampled every 10 s during the gas exposure. In order to evaluate the cross-talk and gas permeability for the composites, several gas streams of varying concentrations of H_2 and CH_4 mixtures in ambient air were pumped into the chamber *via* the mass flow controller. First, H_2 gas streams were pumped with concentrations of 0.5% and 1.0% in ambient air, and to facilitate sensor recovery ambient air was pumped following the two gas cycles. Afterwards, the chamber was filled with streams of 0.5% and 1.0% CH_4 (also in ambient air), similarly followed by ambient air after gas cycles for sensor recovery. Finally, to examine the behaviour of the sensor and the

membrane in mixed gas environment, the mass flow controlled pumped a mixture of 0.5% H_2 and 0.5% CH_4 into the chamber.

Due to the different permeability of the gas species through the membranes exposure times were varied. For the relatively fast gas permeability of H_2, the exposure time was 10 min with a 25 min ambient air recovery in between exposures. CH_4 gas diffusion was relatively slower, and required a longer exposure time of 20 min and 40 min ambient air recovery between exposures.

As the chamber was filled with these gases, the concentrations of the analyte gases that permeated through the different membranes were measured by the commercial sensor. Utilizing the different MWCNT/PDMS membranes in conjunction with the commercial sensor, when exposed to the different concentrations of gas species, the relative normalized permeability ratios for the various composite membranes for different gas species were obtained and demonstrated in Fig. 6. In this graph, all measurements were acquired at room temperature as mentioned previously. The dynamic response of sensing system at different concentrations of gases, used to extract the data presented in Fig. 6, is presented as *Supplementary Information* Fig. S1.

As can be seen in Fig. 6, for different wt% MWCNT/PDMS composites, the response magnitudes and their trends were fairly similar upon exposure to both 0.5% and 1.0% H_2. The permeation of H_2 through the membranes decreased as the concentration of MWCNT increased within the polymer matrix. The permeation of the 0.5% H_2 in ambient air dropped by around 21%, 60%, and 77% through the 1%, 5%, and 10% MWCNT/PDMS composites, respectively. In addition, the permeation of the 1.0% H_2 decreased by approximately 11%, 53%, and 57% through the 1%, 5%, and 10% MWCNT/PDMS composites, respectively.

As can be seen, embedding MWCNT in PDMS considerably attenuated the permeability of the membranes to CH_4. As the concentration of MWCNT increased beyond

1% within the composite material, the membrane almost completely blocked CH_4 diffusion, while allowing the passage of H_2. For the 0.5% CH_4 in ambient air the permeation was attenuated by 96% through 1% MWCNT/PDMS composite and was almost completely blocked at 5% and 10% MWCNT/PDMS composites. The permeation through the 1% MWCNT/PDMS composite of 1% CH_4 dropped by 77% and by around 99% through the 5% and 10% MWCNT/PDMS composites.

It is important to consider that CH_4 molecules are much larger and heavier than H_2 molecules, and as a result their permeations through the membranes take longer. Consequently, CH_4 molecules spend longer time in the membranes, and hence, have a higher chance to interact with the content of the membranes. Additionally, their larger size also increases their chance of interaction with the surroundings. This means that the change in the polymerization and increase in the filler concentration, affect them more significantly than H_2 molecules.

It is observed that H_2 gas molecules permeation also experiences a decrease at higher concentrations of MWCNT. It would be interesting to report the concentration of MWCNT at which a complete blockage of H_2 molecules permeation would occur. However, it is actually not possible to increase the MWCNT concentration in the PDMS/MWCNT composite further than 10%. Due to the dominance of MWCNT over the PDMS part at such concentrations, the membrane cannot be made continuous anymore. As a result, the membrane would have sub-micron or micro-pores that allow the passage of all gases indiscriminately.

As mentioned previously in Section 3.1.2 and revealed from our FTIR analysis (Fig. 3), the intensity of the peak observed at 905 cm^{-1} decreased as the concentration of MWCNT increased in the composite, which corresponds to the formation of Si–C bond. Moreover, with the increase of MWCNT in PDMS, the $Si(CH_3)_2$ rocking peaks appear to

decrease which coincides with an increase in the intensity of Si–H peak. This suggests that these bonds play a significant role in blocking CH_4 through the composite membranes. Similarly, micro-Raman spectra (Fig. 4) from Section 3.1.3, demonstrates the decrease of the $Si–CH_3$ symmetric rocking band as the concentration of MWCNT increases which agrees with the results obtained from FTIR. Additionally, the XPS analysis from Section 3.1.4 shows a decrease in the number of silicon to three oxygen bonds occurring, allowing the increased formation of the Si–C bonds.

We have seen a similar behaviour in the Raman and FTIR spectra of the composites after increasing the concentration of CB fillers [9]. However, there is a striking difference between the behaviour of MWCNT-PDMS and CB-PDMS membranes. CB-PDMS membranes showed blocking of CH_4 only at 6% of CB but the membranes with the higher concentration of CB could not block CH_4. This was associated to the decrease in the number of non-polymerized Si−O and $Si−CH_3$ bonds. Interestingly, the concentration of these bonds increased at higher concentrations of CB in the membranes.

We see the same trend for MWCNT/PDMS composites at low concentration of MWCNT, a decrease in the number of $Si–CH_3$ and Si–O bonds and increase in the number of Si−C bonds. However, for MWCNT composites, increasing the MWCNT concentration above 1% also enhance the blocking of CH_4 even further. This is in agreement with characterization outcomes which confirm that the prevalence of Si−C bonds remain high, even at high concentrations of MWCNT. The most significant difference between CB and MWCNT is the large surface area of MWCNT. While at high concentrations of CB the polymerization of the PDMS onto the surface of carbon was reduced, the same trend was not seen for MWCNTs composites due to the fact that MWCNT have much smaller dimensions, much higher surface activity, and better dispersion in the polymer matrix. These observations

confirm our initial hypothesis predicting better performance of MWCNT as a filler for gas separation membranes.

4. Conclusion

In this work, a number of different weight concentrations of MWCNT in MWCNT/PDMS composite membranes were synthesized (1%, 5% and 10%). The effect of the MWCNT concentration on membrane selectivity towards H_2, and the blockage of CH_4, was studied. It was found that in general the presence of MWCNT in PDMS produced selectivity towards H_2 over CH_4. It was also observed that as the weight ratio of MWCNT increases in PDMS composites, the selectivity to H_2 increased by efficient blocking of CH_4. The advent of selectivity occurred at low MWCNT concentration of only 1% and we ascribed it to the formation of Si–C bonds, a decrease in the number of available Si–CH_3 and Si–O bonds and to some extent the surface reaction of MWCNT with the larger CH_4 molecules in comparison with H_2. Our developed membranes can offer many industrial applications by enabling efficient *in situ* selective H_2 separation from other gas species, with CH_4 demonstrated in our work, using low cost and passive membrane technologies.

Acknowledgements

MN acknowledges the Saudi Arabian Ministry of Higher Education for Financial support. MB and SS acknowledge the Australian Post-Doctoral Fellowships from the Australian Research Council through Discovery Projects DP1092717 and DP110100262, respectively. JDP, SS, and KKZ acknowledge the Australian Research Council for equipment funding through the Linkage, Infrastructure, Equipment, and Facilities Grants LE0989615 and LE100100215.

References

[1] Jung GB, Weng FB, Su A, Wang JS, Yu TL, Lin HL, et al., Nafion/PTFE/silicate membranes for high-temperature proton exchange membrane fuel cells, Int J Hydrogen Energy, 33(2008) 2413-7.
[2] Shao L, Lau CH, Chung TS, A novel strategy for surface modification of polyimide membranes by vapor-phase ethylenediamine (EDA) for hydrogen purification, Int J Hydrogen Energy, 34(2009) 8716-22.
[3] Bernardo P, Drioli E, Golemme G, Membrane gas separation: A review/state of the Art, Ind Eng Chem Res, 48(2009) 4638-63.
[4] Anderson MR, Mattes BR, Reiss H, Kaner RB, Gas separation membranes: A novel application for conducting polymers, Synthetic Met, 41(1991) 1151-4.
[5] Freeman BD, Basis of permeability/selectivity tradeoff relations in polymeric gas separation membranes, Macromolecules, 32(1999) 375-80.
[6] Hong M, Noble R, Falconer J, Highly selective H_2 separation zeolite membranes for coal gasification membrane reactor applications, Technical Report, Univ of Colorado 2004.
[7] Robeson LM, Polymer membranes for gas separation, Curr Opin Solid St M, 4(1999) 549-52.
[8] Li Y, Verbiest T, Vankelecom I, Improving the flux of PDMS membranes via localized heating through incorporation of gold nanoparticles, J Membrane Sci, 428(2013) 63-9.
[9] Nour M, Berean K, Griffin MJ, Matthews GI, Bhaskaran M, Sriram S, et al., Nanocomposite carbon-PDMS membranes for gas separation, Sensors Actuat B-Chem, 161(2012) 982-8.
[10] Bhadra M, Mitra S, Nanostructured membranes in analytical chemistry, Trac-Trend Anal Chem, 45(2013) 248-63.
[11] Safadi B, Andrews R, Grulke EA, Multiwalled carbon nanotube polymer composites: Synthesis and characterization of thin films, J Appl Polym Sci, 84(2002) 2660-9.
[12] Pandey P, Chauhan RS, Membranes for gas separation, Prog Polym Sci, 26(2001) 853-93.
[13] Chung T-S, Jiang LY, Li Y, Kulprathipanja S, Mixed matrix membranes (MMMs) comprising organic polymers with dispersed inorganic fillers for gas separation, Prog Polym Sci, 32(2007) 483-507.
[14] Novak BM, Hybrid nanocomposite materials—between inorganic glasses and organic polymers, Adv Mater, 5(1993) 422-33.

[15] Romasanta LJ, Lopez-Manchado MA, Verdejo R, The role of carbon nanotubes in both physical and chemical liquid–solid transition of polydimethylsiloxane, Eur Polym J, (2013) in press.
[16] Vijay Y, The titanium-coated polymeric membranes for hydrogen recovery, Int J Hydrogen Energ, 27(2002) 905-8.
[17] Kim S, Pechar TW, Marand E, Poly(imide siloxane) and carbon nanotube mixed matrix membranes for gas separation, Desalination, 192(2006) 330-9.
[18] Sanip SM, Ismail AF, Goh PS, Soga T, Tanemura M, Yasuhiko H, Gas separation properties of functionalized carbon nanotubes mixed matrix membranes, Sep Purif Technol, 78(2011) 208-13.
[19] Kim S, Jinschek JR, Chen H, Sholl DS, Marand E, Scalable fabrication of carbon nanotube/polymer nanocomposite membranes for high flux gas transport, Nano Lett, 7(2007) 2806-11.
[20] Ghadimi A, Sadrzadeh M, Mohammadi T, Prediction of ternary gas permeation through synthesized PDMS membranes by using principal component analysis (PCA) and fuzzy logic (FL), J Membrane Sci, 360(2010) 509-21.
[21] Park SS, Tatum CE, Lee Y, Dual electrochemical microsensor for simultaneous measurements of nitric oxide and oxygen: Fabrication and characterization, Electrochem Commun, 11(2009) 2040-3.
[22] Zhan X, Pervaporation properties of PDMS membranes cured with different cross-linking reagents for ethanol concentration from aqueous solutions, Chinese J Polym Sci, 27(2009) 533.
[23] Atayde C, and Doi I, Highly stable hydrophilic surfaces of PDMS thin layer obtained by UV radiation and oxygen plasma treatments, Phys Status Solidi C, 7(2010) 189-92.
[24] Lötters J, Olthuis W, Veltink PH, and Bergveld P, The mechanical properties of the rubber elastic polymer polydimethylsiloxane for sensor applications, J Micromech Microeng, 7(1997) 145.
[25] Merkel TC, Bondar VI, Nagai K, Freeman BD, Pinnau I, Gas sorption, diffusion, and permeation in poly(dimethylsiloxane), J Polym Sci Pol Phys, 38(2000) 415-34.
[26] Nakagawa T, Nishimura T, Higuchi A, Morphology and gas permeability in copolyimides containing polydimethylsiloxane block, J Membrane Sci, 206(2002) 149-63.
[27] Ismail AF, Goh PS, Sanip SM, Aziz M, Transport and separation properties of carbon nanotube-mixed matrix membrane, Sep and Purif Technol, 70(2009) 12-26.

[28] Liu P-T, Tsai CT, Chang TC, Kin KT, Chang PL, Chen CM, et al., Activation of carbon nanotube emitters by using supercritical carbon dioxide fluids with propyl alcohol, Electrochem Solid-State Lett, 9(2006) 124-6.
[29] Marinkovic SN, Review carbon nanotubes, J Serb Chem Soc, 8–9(2008) 891–913.
[30] Serp P, Corrias M, Kalck P, Carbon nanotubes and nanofibers in catalysis, Appl Catal A-Gen, 253(2003) 337-58.
[31] Zeng Y, Liu P, Du J, Zhao L, Ajayan PM, Cheng H-M, Increasing the electrical conductivity of carbon nanotube/polymer composites by using weak nanotube–polymer interactions, Carbon, 48(2010) 3551-8.
[32] Ahir SV, Huang YY, Terentjev EM, Polymers with aligned carbon nanotubes: Active composite materials, Polymer, 49(2008) 3841-54.
[33] Battie Y, Ducloux O, Patout L, Thobois P, Loiseau A, Selectivity enhancement using mesoporous silica thin films for single walled carbon nanotube based vapour sensors, Sensors Actuat B-Chem, 163(2012) 121-7.
[34] Maji D, Lahiri SK, Das S, Study of hydrophilicity and stability of chemically modified PDMS surface using piranha and KOH solution, Surf Interface Anal, 44(2012) 62-9.
[35] Owen MJ, Dvornic PR, Silicone Surface Science: Springer Netherlands; 2012.
[36] Agarwal R, Tandon P, Gupta VD, Phonon dispersion in poly(dimethylsilane), J Organomet Chem, 691(2006) 2902-8.
[37] Bodas D, Khan-Malek C, Formation of more stable hydrophilic surfaces of PDMS by plasma and chemical treatments, Microelectron Eng, 83(2006) 1277-9.
[38] Bae SC, Lee H, Lin Z, Granick S, Chemical imaging in a surface forces apparatus: Confocal raman spectroscopy of confined poly(dimethylsiloxane), Langmuir, 21(2005) 5685-8.
[39] Costa S, Borowiak-Palen E, Kruszynska M, Bachmatiuk A, Kalenczuk RJ, Characterization of carbon nanotubes by Raman spectroscopy Mater Sci-Poland, 26(2008) 433-41.
[40] Dresselhaus MS, Dresselhaus G, Saito R, Jorio A, Raman spectroscopy of carbon nanotubes, Phys Rep, 409(2005) 47-99.
[41] Osswald S, Havel M, Gogotsi Y, Monitoring oxidation of multiwalled carbon nanotubes by Raman spectroscopy, J Raman Spectrosc, 38(2007) 728-36.
[42] Eklund PC, Holden JM, Jishi RA, Vibrational modes of carbon nanotubes; Spectroscopy and theory, Carbon, 33(1995) 959-72.

[43] Narimissa E, Gupta R, Bhaskaran M, and Sriram S, Influence of nano-graphite platelet concentration on onset of crystalline degradation in polylactide composites, Polym Degrad Stab, 97(2012) 829–32.
[44] Zhang H-B, Lin G-D, Zhou Z-H, Dong X, Chen T, Raman spectra of MWCNTs and MWCNT-based H2-adsorbing system, Carbon, 40(2002) 2429-36.
[45] McNally T, Pötschke P, Halley P, Murphy M, Martin D, Bell SEJ, et al., Polyethylene multiwalled carbon nanotube composites, Polymer, 46(2005) 8222-32.
[46] F. Tuinstra JLK, Raman spectrum of fraphite, J Chem Phys, 53(1970) 1126-30.
[47] Akhavan O, The effect of heat treatment on formation of graphene thin films from graphene oxide nanosheets, Carbon, 48(2010) 509-19.
[48] Muehlhoff L, Choyke WJ, Bozack MJ, Yates JT, Comparative electron spectroscopic studies of surface segregation on SiC(0001) and SiC(0001), J Appl Phys, 60(1986) 2842-53.
[49] Beamson G, Briggs D, High resolution XPS of organic polymers : the Scienta ESCA300 database, Chichester [England]; New York: Wiley; 1992.
[50] Finster J, Klinkenberg ED, Heeg J, Braun W, ESCA and SEXAFS investigations of insulating materials for ULSI microelectronics, Vacuum, 41(1990) 1586-9.
[51] Morra M, Occhiello E, Marola R, Garbassi F, Humphrey P, Johnson D, On the aging of oxygen plasma-treated polydimethylsiloxane surfaces, J Colloid Interf Sci, 137(1990) 11-24.

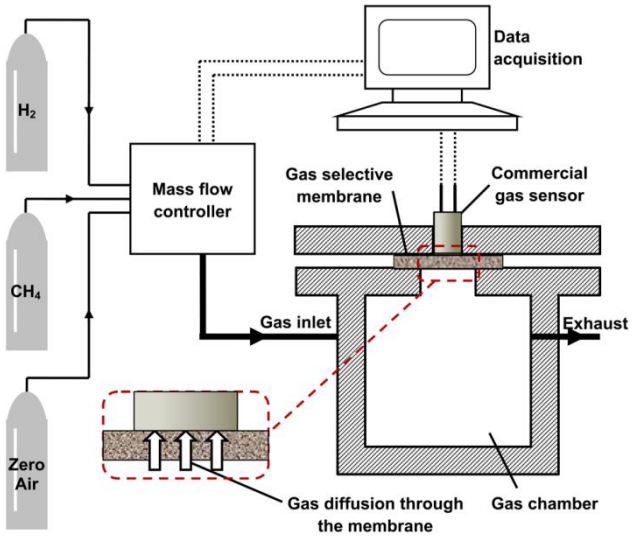

Fig. 1. Schematic of the gas sensing setup illustrating the gas sensing module and location of the gas selective membrane (not to scale).

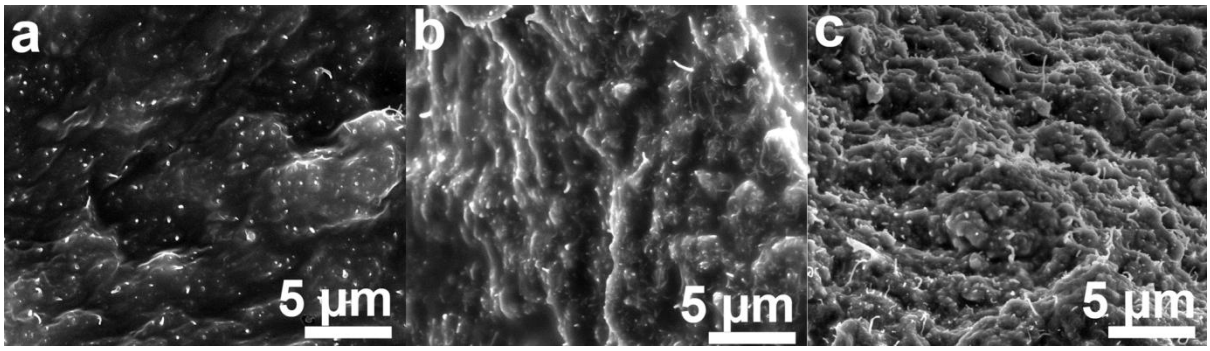

Fig. 2. Cross sectional SEM images of MWCNT/PDMS nanocomposite membranes of different concentrations, showing the bundle distributions for MWCNT weight concentrations of: (a) 1%; (b) 5%; and (c) 10%.

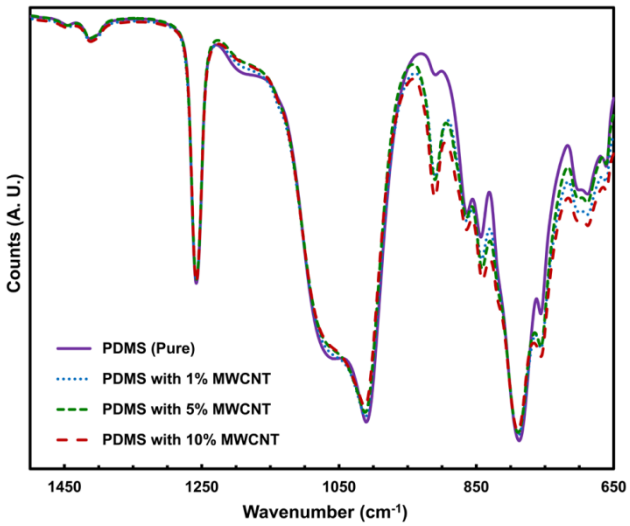

Fig. 3. FTIR spectra for the pure PDMS and MWCNT/PDMS nanocomposite membranes.

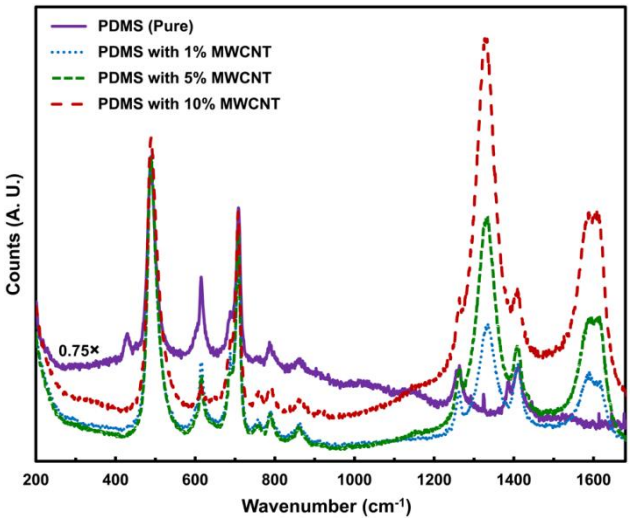

Fig. 4. Micro-Raman spectra for: pure PDMS and three different MWCNT concentrations in MWCNT/PDMS nanocomposite membranes.

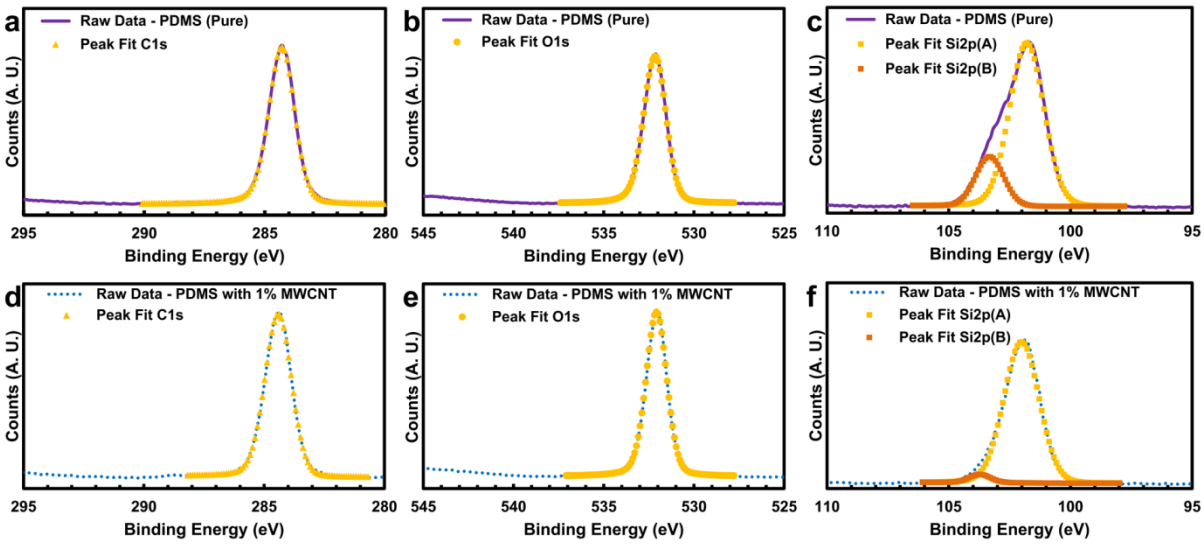

Fig. 5. XPS analysis results: (a)-(c) show C, O, and Si peaks for the pure PDMS, respectively. (d)-(f) show C, O, and Si peaks for the 1% MWCNT /PDMS, respectively.